Eur. Phys. J. Special Topics **227**, 1681–1692 (2019)

https://doi.org/10.1140/epjst/e2019-800157-0

THE EUROPEAN PHYSICAL JOURNAL SPECIAL TOPICS

Regular Article

Diamondoid-functionalized nanogaps: from small molecules to electronic biosensing

Frank C. Maier[1], Chandra S. Sarap[1], Maofeng Dou[1], Ganesh Sivaraman[1,2], and Maria Fyta[1,a]

[1] Institute for Computational Physics, University of Stuttgart, Allmandring 3, 70569 Stuttgart, Germany
[2] Argonne Leadership Computing Facility, Argonne National Laboratory, Argonne, Illinois 60439, USA

Received 1 October 2018 / Received in final form 25 October 2018
Published online 8 March 2019

Abstract. The potential of reading-out DNA molecules using functionalized electrodes embedded in nanopores is discussed here. Focus is given on functionalization using tiny diamond-like hydrogenated cages, the diamondoids. A derivative known as memantine of the smallest diamondoid is taken. This offers hydrogen bonding possibilities. Based on quantum-mechanical calculations, we first assess the interaction details of memantine with DNA units, the nucleotides. At a next step, nucleotides are placed within the nanogap formed by the diamondoid-functionalized electrodes. Quantum transport calculations are performed and show the high sensitivity of the electrodes in distinguishing among the different nucleotide types. We proceed by qualitatively revealing the influence of the DNA molecules by simply rotating the nucleotide within the nanogap. The effect of an aqueous environment is also included and the dynamic behavior of the conductance across the functionalized electrodes is addressed. In the end, we discuss the relevance of our results in detecting DNA sequences.

1 Introduction

Sensing biomolecules, such as DNA is essential for detecting their sequences and is highly relevant to medical care and therapy design. One of the novel sequencers, the so called "next generation sequencing platforms" involves nanopores. The latter are nanometer-sized holes in materials and have the ability to detect DNA [1–5]. A nanopore can electrophoretically thread a biomolecule within a salt solution realizing single-molecule experiments [6]. In order to not only detect the passage of a DNA through the pore, but also read-out its exact sequence, different protocols have been proposed. One of these is the use of transverse tunneling currents [7,8]. This read-out technique requires that metallic electrodes are embedded into the nanopore. Applying a voltage difference across these would result an electronic current expected to distinguish among the DNA nucleotides passing through the nanopore. Although this is a very promosing technique, often the tunneling signals for the four nucleotides overlap

[a] e-mail: mfyta@icp.uni-stuttgart.de

leading to a low signal-to-noise ratio [9,10]. Enhancing the nucleotide-specificity of these signals could be possible through a functionalization of the nanopores [1,11]. In functionalized nanopores, the metallic electrodes embedded in the nanopore are functionalized by molecules of the size of the nucleotides, interacting with the nucleotides through hydrogen bonds. This interaction is expected to give rise to highly nucleotide specific electronic signals. These signals are expected to also detect DNA mutations, that is distinguish "healthy" nucleotides from modified ones. Detection technologies have been improving along these lines as well [12–15]. Being able to read-out mutations or modifications in DNA molecules can be a keystone in revolutionizing cancer therapies [16].

In this respect and in nanopore sensors, the choice of the functionalizing molecule is of high importance. Based on a good choice of these molecules, functionalization in the nanopore has the potential to enhance the transverse signals across the nanopore [11,17]. Nevertheless, it is crucial to find molecules of the size of the DNA nucleotides, which can functionalize nanopores and indeed increase the signal-to-noise ratio in the electronic current measurements. Such an increase is required to facilitate an almost error-free reading-out of the DNA nucleotides and promote sequencing. It has been previously shown that the use of a small diamond-like molecule known as diamondoid can indeed enhance the read-out signals [18]. Diamondoids are nanoscale diamond-like carbon nanocages, which are terminated by hydrogen atoms, are thermodynamically very stable, have tunable properties, can be selectively tuned, and come in a variety of sizes and modifications [19–24]. For the functionalization of the electrodes, derivatives of diamondoids [25,26] can offer grafting possibilities to the metallic surface of the electrode, and additional donor/acceptor sites for binding to the DNA. Indeed, it has been shown that derivatives of diamondoid form hydrogen bonds to DNA nucleotides [27].

Here, we further investigate the relevance for biosensing of one of the smallest diamondoid derivatives, known as memantine [28]. Memantine is bio-compatible and well known as a drug used in Alzheimer's disease [29,30]. This molecule will be taken here as a potential candidate for detecting DNA in a functionalizing gold electrode gap. We provide a detailed study, starting from the specific interactions of memantine to DNA nucleotides, both canonical and modified and move up to conductance of the memantine-functionalized gap and its dependence on the DNA dynamics. The identification of mutations and epigenetic markers with such a sensor gap is also addressed in order to provide a better understanding of the inherent characteristics of the detection properties of canonical and modified DNA units. To this aim, we use computer simulations and model the interaction of diamondoids and DNA and the electronic transport across the electrodes. The latter will be a measure of the detection efficiency. This paper is organized as follows: in Section 2 the methods used are described, in Section 3 the results are discussed, while a summary is given in Section 4.

2 Methodology

The main objective of the current study is to test a certain diamondoid as a probe to interrogate and identify DNA nucleotides, as well as to differentiate the canonical nucleotides from their modified counterparts. This diamondoid, memantine will be functionalized with a thiol group that provides the anchor to an electrode material. We will use the notation "memS" for the thiol-functionalized memantine. For the DNA part, the four natural DNA nucleotides (i.e. nucleobases with the sugar phosphate backbone), namely 2′-deoxyadenosine 5′-monophosphate, 2′-deoxythymidine 5′-monophosphate, 2′-deoxycytidine 5′-monophosphate, 2′-deoxyguanosine

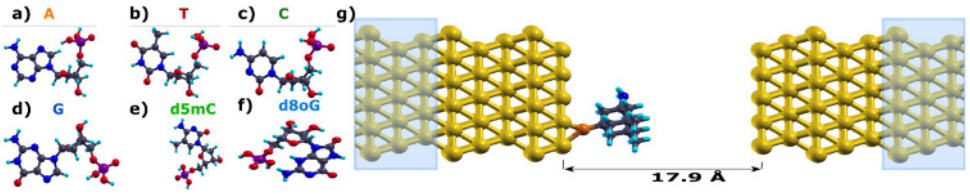

Fig. 1. The nucleotides used in this work are shown on the left: A, T, C, G, d5mC and d8oG. The hydrogen, carbon, nitrogen, oxygen, phosphorus, and thiol atoms are colored in white, cyan, blue, red, tan, and yellow, respectively. Panel g: depicts the functionalized nanogap. The functionalizing molecule memS is visible on the left electrode. The gold electrodes and the thiol group for grafting the memS on the left electrode are shown in yellow and orange, respectively. In this setup the electronic current can flow from the left to the right electrode though electron tunneling. The same color coding as in this figure will be used throughout.

5′-monophosphate and the two mutants, 2′-Deoxy 5′-methylcytidine and 8′-oxo 2′-deoxyguanosine 5′-monophosphate are considered here. For simplicity, these are represented as "A", "T", "C", "G", "d5mC" and "d8oG", respectively. The geometries of all the isolated molecules, nucleotides and diamondoid, are optimized as will be described in this section and the resulting structures are presented in Figure 1.

All simulations are performed within the density functional theory (DFT) approach. The geometry optimizations for the diamondoids, nucleotides and the diamondoid-nucleotide complexes are performed using the density functional theory as implemented in Gamess-US [31,32] and SIESTA [33]. For the interactions of memS and each nucleotide, dispersion-including DFT with a Pople basis set of polarized triple-ζ basis functions is employed. The ground-state electronic properties are carried out using the M06-2X functional [34]. This functional has been successfully applied for describing the interactions of nucleobases with graphene and carbon nanotubes [35,36]. The initial geometry optimization of the structures are performed using the 6-31G(d,p) basis set, followed by single-point energy calculations at the 6-311+G(d,p) level with the same functional (M06-2X/6-311+G(d,p)//M06-2X/6-31G(d,p)). The vibrational frequency analysis is carried out to ensure that the obtained geometries represent the minimum-energy configuration on the potential energy surface. MemS and a nucleotide are brought together in two different arrangements.

As the nucleobases are aromatic in nature and the memS contains hydrogen-terminated sp^3 carbons along with the $-NH_2$ and $-SH$ substitution groups, the interactions are purely non-covalent and are governed by CH...π, NH...π, and SH...π interactions besides the predominant hydrogen bonding interactions. The latter interaction is stronger and can potentially be used for sensing purposes [18,37]. For sensing, memS will be attached to metallic electrodes through its thiol group, which in turn cannot take part to the binding with a nucleotide. To this aim, we focus only on the hydrogen bonding configurations. Typically, a propeller angle can be defined to study the hydrogen bonding strengths within DNA base-pairs and elude the $\pi-\pi$ stacking due to the van der Waals interactions [38]. A similar approach is used here by aligning the $-NH_2$ group of memS with respect to the nucleotides. As a measure of the binding strengths between the diamondoid and the nucleotide, the hydrogen-bond interaction energy is computed as

$$\Delta E_{\mathrm{hb}} = E_{\mathrm{complex}} - E_{\mathrm{memS}} - E_{\mathrm{nucleotide}}, \tag{1}$$

where E_{memS} and $E_{\mathrm{nucleotides}}$ are the energies of the isolated diamondoid and the isolated nucleotide in the corresponding complexes, respectively. E_{complex} is the energy of the memS-nucleotide complexes. The E_{int} are corrected for the basis set superposition error using the counterpoise method [39].

In order to compute the electron transport properties of the memS-functionalized electrodes depicted in Figure 1g, the gold electrodes are considered and represented by a single-zeta plus polarization basis set, the remaining atoms are represented by double-zeta plus polarization basis set. The exchange-correlation functional is approximated by the Perdew–Burke–Ernzerhof (PBE) functional [40]. The fineness of the real-space grid, the mesh-cutoff, is set to 200 Ry. During the structural relaxation, the integration over k-space is performed with $4 \times 4 \times 1$ k-points. For the calculation of the electronic properties and transport properties we used a k-space of $5 \times 5 \times 1$ k-points. The structural relaxation was performed until the maximum atomic forces reached less than $0.01\,\mathrm{eV\,\AA^{-1}}$. The supercell of $14.8 \times 14.8 \times 39.7\,\mathrm{\AA}$ consists of two gold electrodes (111), each represented by 5×5 gold atoms in 5 layers each. The diamondoid memantine and one nucleotide are placed in the 18 Å wide gap between both electrodes in such a way, that the phosphate group of the nucleotide is oriented close to the right electrode and the diamondoid attached to the left electrode by a sulfur atom. For the investigation of DNA dynamics effects, the nucleotide is rotated at increments of 20° along the axis connecting both electrodes. At each rotation, both the diamondoid and the nucleotide are relaxed. All transport calculations were performed using the nonequilibrium Green's function method (NEGF), implemented in TRANSIESTA [41]. For post-processing and the calculation of the transmission spectra, we used TBTrans with a finer k-point sampling of $10 \times 10 \times 1$ k-points. The electronic transmission was calculated at zero bias.

At the final step of this investigation, the influence of an aqueous environment in the memS-functionalized device is examined. For this, a Quantum Mechanics (QM) and Quantum Mechanics/Molecular Mechanics (QM/MM) approach is taken as implemented in the code CP2K [42]. In order to benchmark the approach, first full QM calculations were performed and taken as references for a comparison to the QM/MM results. The DNA nucleotides, water solvent, and diamondoid are calculated at the QM level. At this level, DFT is applied with the core electrons being described through norm-conserving Goedeker–Teter–Hutter (GTH) pseudopotentials [43,44]. The valence electrons are represented using double-ζ valance plus polarization (DZVP) basis sets of Molopt-type [45]. The exchange-correlation interactions are described through the PBE functional [40]. Van der Waals interactions are accounted for by employing Grimme's D3 dispersion correlation [46]. The energy cut off for the auxiliary plane wave is set to 300 Ry. The Brillouin zone integration is performed using a Monkhorst-Pack scheme with $1 \times 1 \times 1$ grid for the k-points. Within our QM/MM calculations, the Au electrodes are modelled at the MM level. For the interactions therein, the embedded atom model (EAM) potential [47] as obtained from the LAMMPS database [48] is applied. The interactions between Au, water, DNA nucleotides, and diamondoid are modeled using Lennard-Jones potentials with parameters from reference [49]. For the QM/MM boundary across the Au-S covalent bond, the integrated molecular orbitals/molecular mechanics (IMOMM) [50,51] approach is applied to describe the frontier orbitals and the valence electrons of the QM region are compensated by adding a F atom. The electrostatic screening effect of the Au electrodes is described using the image charge approach [52], where the charge distribution induced in the Au electrode is modeled by a set of Gaussian ("image") charges centered at the Au atoms. The size of the supercell is set to $14.806 \times 14.806 \times 19.963$ Å, which contains 60 water molecules. In order to prevent the DNA nucleotide drifting away from diamondoid, one carbon atom on the backbone of DNA nucleotide is kept fixed throughout the QM/MM simulation. The Molecular Dynamics part of the QM/MM simulations are first performed in the microcanonical (NVE) ensemble at 300 K with time step of 0.5 fs for a duration of 20 ps. This serves as a thermalization step. These simulations are followed by further Molecular Dynamics

simulations for another 10 ps in the canonical (NVT) ensemble with a velocity-rescaling thermostat. The trajectories of the last 10 ps under the (NVT) ensemble are used for the analysis. These are saved every 1 ps for the electronic structure calculations.

3 Results and discussion

We proceed with the discussion of the results, which are divided as follows: at first the details on the hydrogen bonding interactions of memS and a nucleotide in two different arrangements will be given. The hydrogen bond distances, energies, electronic band-gap, and optical absorption of these complexes are provided. Having verified the interactions and characteristics of a memS-nucleotide complex, we move on with functionalizing one gold electrode with the memS molecule. All four nucleotides and their two modifications are separately placed within the functionalized electrode gap in order to evaluate the electronic transmission across this nanogap. At a next step, one of the nucleotides is rotated within the nanogap in order to reveal its dynamic effects on the electronic transmission. In the end, water is taken to fill in the nanogap and the electronic conductance across the functionalized electrodes is evaluated.

3.1 Diamondoid-nucleotide complex: interactions

We begin with the analysis of the memS-nucleotide complexes, and show the optimized geometries for two different arrangements within the memS-C complex in Figure 2. In Figure 2a, the amine group of memS acts as a hydrogen bond acceptor ("H-bond acceptor") and it is stabilized by three hydrogen bonds. In order to confirm that the memS with $-NH_2$ group as an H-bond acceptor forms the minimum energy configurations with the nucleotides, we also consider memS-nucleotide complexes in which the memS $-NH_2$ group acts as a hydrogen bond donor ("H-bond donor") as in Figure 2b. The hydrogen bond characteristics of all the diamondoid-nucleotide complexes, including the interaction energies, hydrogen bond distances and the electronic band gaps for H-bond acceptor and H-bond donor configurations are summarized in Table 1. In all cases, memS and the nucleotides are kept together at relatively short distances having considerable interaction energies. These vary among the complexes, with the memS-A complex having the lowest interaction energy in its H-bond acceptor arrangement, while the memS-d8oG complex seems to be the less stable in its H-bond donor arrangement. Overall, the H-bond acceptor configurations have the higher interaction energy justified by the fact that more hydrogen bonds are formed, so that memS and the nucleotide are kept together at a shorter distance. A nucleotide specific dependence in the electronic energy gap was observed without revealing specific trends [53].

As a property indicative of the nucleotide specificity in the complexes, we compute their absorption spectra using the linear response time-dependent density functional theory (LR-TDDFT). For the memS-C complex in both arrangements, these are shown in Figure 2c and are compared to the isolated memS and C. The computed absorption spectra for all nucleotides (not shown) are in the range of 5–8 eV. The observed trends agree well with the experiments taking into account a shift of about 1 eV [54,55]. From Figure 2 it can be inferred that the spectral range for the isolated memS and the cytosine is similar. Interestingly, a slight shift in the absorption spectra can be seen for the complex. We have also observed a decrease in the oscillator strengths for all complexes at a higher energy related to the pronounced peak of

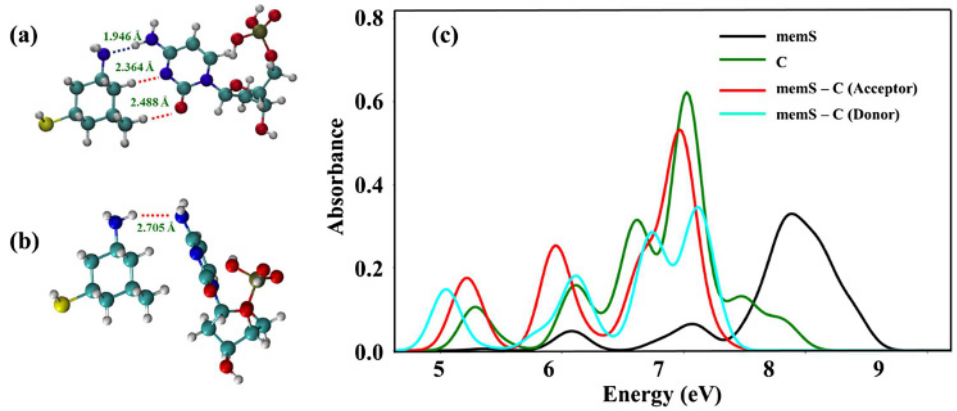

Fig. 2. The (a) acceptor and (b) donor configurations for the memS-C complex are shown. The graph in panel (c) depicts the absorption spectra of these two bonding configurations and compared to those of the isolated memS and C, respectively.

Table 1. The hydrogen bonding characteristics, interaction energy $\Delta E_{\rm hb}$ (in kcal mol^{-1}) and bond distance $r_{\rm hb}$ (in Å), and the respective electronic band gap $E_{\rm g}$ (in eV) for the diamondoid-nucleotide complexes.

Complex	H-bond acceptor			H-bond donor		
	$\Delta E_{\rm hb}$	$r_{\rm hb}$	$E_{\rm g}$	$\Delta E_{\rm hb}$	$r_{\rm hb}$	$E_{\rm g}$
memS-A	−10.20	1.973	7.85	−7.88	2.523	7.74
memS-T	−11.62	1.790	7.64	−10.26	2.649	7.83
memS-C	−12.75	1.946	7.79	−6.77	2.705	7.46
memS-G	−15.07	2.438	7.49	−7.92	2.578	7.62
memS-d5mC	−12.52	1.941	7.76	−12.47	2.012	7.68
memS-d8oG	−15.32	2.532	7.36	−5.36	2.748	7.45

the isolated memS. At these higher energies memS is significantly interacting with the nucleotides. The features in the absorption spectra of the memS-C complexes are dominated by cytosine. This is essentially due to the presence of electron-rich parts in cytosine (in comparison to memS) and these participate in the electronic excitation. Similar are the observations for all complexes investigated here.

3.2 Electronic transport across the nanogap

Having unravelled the properties for the memS-nucleotide complexes, we move on by grafting the memS molecule onto the surface of the left electrode and placing a nucleotide one at a time into the functionalized gap shown in Figure 1g. For this part, we only consider one arrangement of the nucleotide relative to the memantine. The electronic transport calculations reveal the electronic transmission characteristics across the functionalized device. These are summarized for all complexes in Figure 3. Sharp peaks with a strength close to 1, at different energies for each nucleotide are observed in the transmission $T(E)$ spectra. The projected density of states (not shown here) for these systems reveal that the higher contribution to each peak arises from the nucleotide suggesting clear nucleotide fingerprints in the functionalized electrode transport properties. At the Fermi level, the hierarchy in the electronic transmission follows the trend d5mC > C > G ≈ T > A > d8oG with variations of up

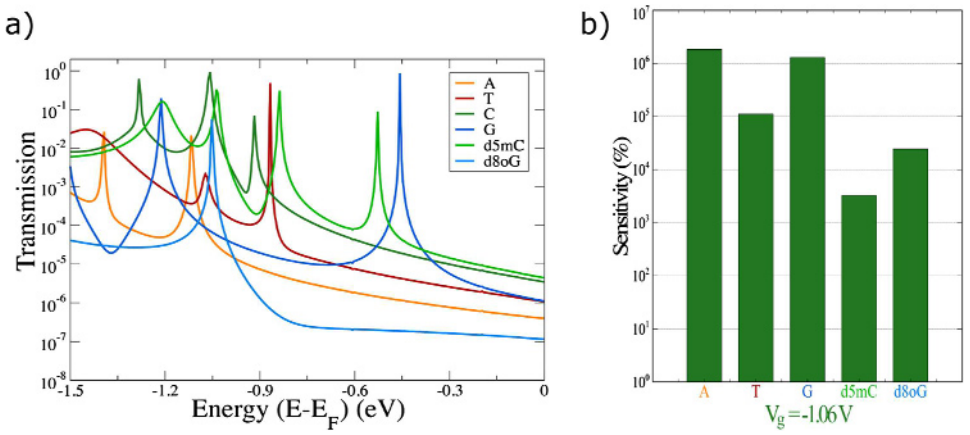

Fig. 3. (a) The transmission spectra with respect to the electronic energy (shifted so that the Fermi energy (E_F) lies at zero eV) for the six nucleotides (the canonical A, T, C, G, and the modified d5mC and d8oG). (b) A bar plot of the sensitivity in detecting C with respect to all other nucleotides.

to two orders of magnitude. This can be translated into a distinguishability of the nucleotides at the Fermi level, i.e. a zero gate voltage. At this level, A and d8oG will be clearly distinguishable, but the other nucleotides might show almost overlapping signals. Nevertheless, the epigenetic d8oG should be efficiently distinguished from its "healthy" counterparts, G. The differences between d5mC and C are much smaller.

In view of sensing the identity of the nucleotide, the Fermi level should be tuned to the nucleotide peaks. In the experiments, this will be possible though applying an external gate. In this respect, a gating conductance g (for a small bias) can be defined as a function of the gate voltage, V_g as $(g(V_\mathrm{g}) = G_0 T(\mu))$, where $\mu = E_F - eV_\mathrm{g}$, T the transmission function, and $G_0 = \frac{2e^2}{h}$ the conductance quantum [56]. Accordingly, in order to read-out DNA, a reference system is needed having a specific gating conductance g_ref that corresponds to the transmission peak of a specific nucleotide at a gating voltage V_g. Taking as g_x the gating conductance, at the same gate voltage for any other nucleotide apart from the reference nucleotide can allow the identification of the nucleotide through the sensitivity

$$S(V_\mathrm{g})[\%] = \left| \frac{g_\mathrm{ref} - g_x}{g_x} \right| \times 100. \tag{2}$$

This can serve as a quantitative measure of how well resolved the conductance of the reference nucleotide will be with respect to other nucleotides. The device sensitivity taking C as a reference at a gating voltage of $V_\mathrm{g} = -1.06\,\mathrm{V}$ (corresponding at a strong resonance peak for C) is given as a bar chart in Figure 3b. It is evident from this figure, that the sensitivity of the device in recognizing C is at least five orders of magnitude higher than the other natural nucleotides (A, T, and G). We can thus infer that at this gating voltage, the device could clearly identify C. At this gating, C can also be 3 times better resolved from its mutated counterpart, d5mC. These results suggest a clear identification of the nucleotides and their modifications based on a proper tuning of the device characteristics.

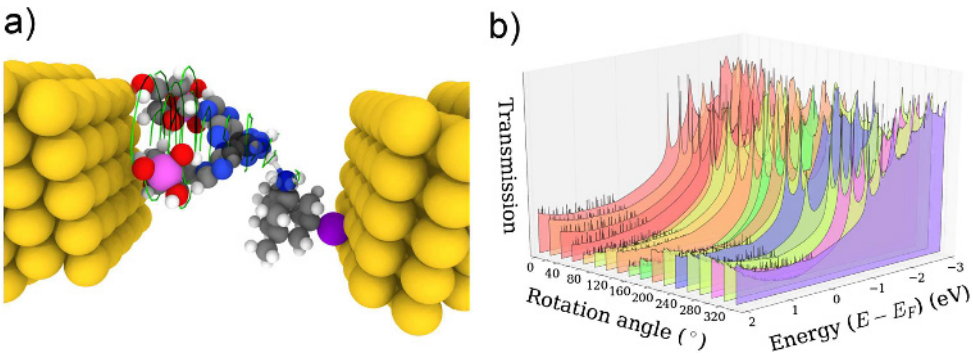

Fig. 4. (a) A sketch showing the rotation details (green traces) of A within the nanogap. (b) A 3D plot showing the variation in the transmission spectra with respect to the rotation angle and the electronic energy shifted so that the Fermi energy (E_F) lies at zero eV.

3.2.1 Influence of DNA dynamics and solvent

The results in Figure 3 refer to *in vacuo* calculations in which the nucleotide is kept fixed in the nanogap. In reality, DNA is a flexible molecule moving in a salt solution. In order to account – at a first approximation – these effects, we discuss them in two steps. First, we include some dynamics effects by simply rotating the nucleotide along the transport direction in the functionalized nanogap, while preserving the hydrogen bond associated with the diamondoid. Taking adenine as a representative nucleotide, this is rotated within the nanogap as indicated by the green traces in Figure 4a. The rotation of the nucleotide was performed in increments of 20° steps. The corresponding transmission for each rotation step is visualized in Figure 4b where the energy is given with respect to the Fermi level set at 0 eV. In this panel, the transmission axis is logarithmically scaled, while no voltage bias is applied. From these data it can be observed that clear resonance peaks remain throughout the rotation and slightly shift relative to the energy range of the resonance peak for no rotation, i.e. zero degrees. This indicates again possible tuning by means of a gating voltage. At the Fermi level corresponding to no gating, the strength of the transmission peaks is rotation dependent. These results, though do unveil a specific trend in the influence of the rotation. Additional investigation is currently being carried out for all nucleotides in order to quantify the effect of dynamics. Note, that the integral over the transmission in the range $\left[-\frac{V_{\text{bias}}}{2}, +\frac{V_{\text{bias}}}{2}\right]$ provides a rough indication of the current generated by a voltage bias V_{bias} applied across the electrodes. However, an applied bias would influence directly the transmission spectra. In this respect, a more in depth investigation would be needed to quantify the combined DNA dynamics and nucleotide specific applied bias effects on the electronic current across the functionalized
gap.

As a final step, we include the influence of the solvent and related thermal fluctuations on the characteristics of the functionalized electrodes through the QM/MM calculations. A snapshot of this system is depicted in Figure 5a in the case of cytosine. The simulations revealed that the water molecules tend to move towards the gold electrodes. Due to the reorientation of the water molecules arising from the polarization induced by the image charges, some hydrogen atoms are pointing towards the gold surfaces. Our results also indicate that the water molecules are weakly bonded to the backbone of the nucleotide. In the case of memS, this shows a more hydrophobic behavior, as the average distance between the hydrogen further away from the center of mass of the molecule and that of water oxygen is about 2.8 Å. This further indicates

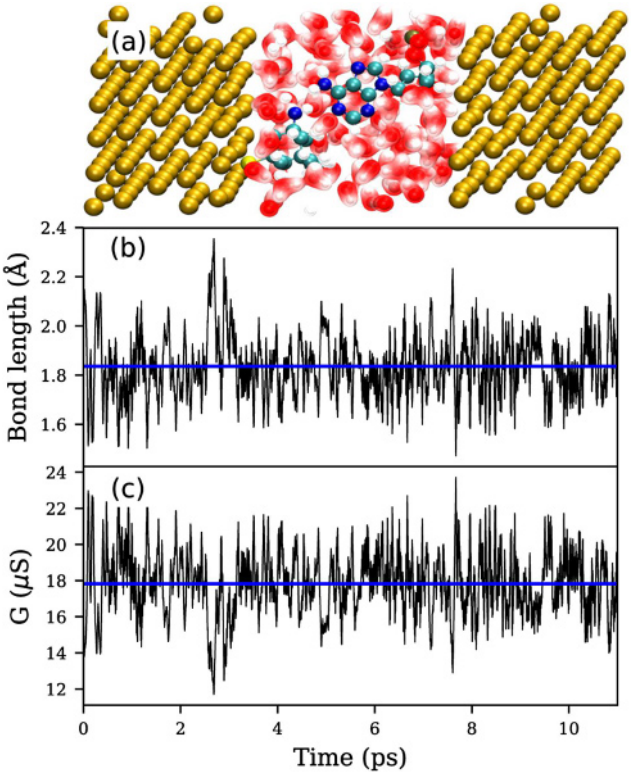

Fig. 5. (a) The memS-functionalized electrodes including cytosine and water molecules. The latter are depicted in white (hydrogen) and red (oxygen). (b) The dynamic evolution of the hydrogen bond distance d_{hb} with time. (c) The corresponding time evolution of the nano-gap conductance derived from equation (3). The solid blue line indicates the time averaged values in both the hydrogen bond length and the conductance.

that the diamondoid tends to repel water and in this way reduce the noise arising from water thermal fluctuations. The distance between cytosine and the diamondoid increases compared to that without water solvent. When the water is included, the distance between the water hydrogen and a nitrogen atom in C is about 2.1 Å.

The hydrogen bond distance d_{hb} between memS and the nucleotide is also strongly fluctuating with time as indicated in Figure 5b. This distance can be directly correlated to the conductance across the nanogap [57], according to

$$G = G_0 \exp(-\beta d_{\mathrm{hb}}), \tag{3}$$

where β is the electronic decay constant, which we have found from the hydrogen bond characteristics of the memS-nucleotide complexes studied in the first part of this work equal to $0.8\,\text{Å}^{-1}$. Specifically, based on our calculations and analysis on the hydrogen bonding within the complex, this parameter was the optimal one mapping the inverse distance at which the hydrogen bonding, i.e. the interaction energy of the diamondoid and the nucleotide, becomes very weak. Accordingly, the time evolution of the conductance across the functionalized electrodes can be calculated though this equation. The results are given in Figure 5c and indicate that the variations in the hydrogen bond length result in larger variations in the conductance due to the exponential relation in Figure 3. Evidently, larger peaks in the conductance arise from stretching of the memS-C hydrogen bonds. The time-averaged values of this

hydrogen bond length and the conductance were calculated at 1.84 Å and 17.82 μS, respectively. The fact that the conductance remains relatively constant with time when water is included, indicates that even in this case the nucleotides can be distinguished by time averaging.

4 Summary and conclusions

In this work, using quantum-mechanical calculations, we discuss the potential and inherent characteristics of functionalized electrodes, which can be embedded in sensing nanopores. The functionalization is based on derivatives of small diamond-like cages, the diamondoids. As a first step towards these biosensing devices, we had to investigate whether the diamondoid derivatives do form relatively strong hydrogen bonds to the DNA units, i.e. the nucleotides. Based on DFT calculations, we could reveal a strong bonding, which was found to be dependent on the relative arrangement of the diamondoid and the nucleotide molecules. The optical spectra of these molecules are nucleotide specific and showed small relative shifts for the two arrangements. The strong hydrogen-bonding of the two molecules set the basis to further use the diamondoid to functionalize one of the electrodes.

In order to evaluate whether these electrodes can potentially detect the identity of DNA nucleotides, we have separately placed the four canonical nucleotides in the electrode gap. For these we have calculated the electronic transport across the electrodes and found strong nucleotide specific peaks in the electronic transmission. Accordingly, our functionalization choice indeed increases the signal-to-noise ratio in the electronic current measurements. Such an increase is required to facilitate an almost error-free reading-out of the DNA nucleotides and promote sequencing. Placing two modified nucleotides, a mutation and an epigenetic marker within the diamondoid-functionalized electrodes revealed additional interesting features. Based on these, it was made clear that such a device can clearly distinguish between a canonical nucleotide and its mutations. In order to quantify this, we have introduced the sensitivity of the device denoting how well resolved each nucleotide is at certain transmission peaks. Up to this point, our calculations on the functionalized electrodes were done for a specific relative arrangement of the molecules. As a simple test of how the dynamics would influence the whole picture, we have rotated the nucleotide in the electrode gap in a simple way by leaving the backbone part always parallel to one of the electrodes. This allowed us to evaluate the dependence of the electronic transmission on the rotation angle. The transmission peaks remained strongly localized in the same energy window, while their relative strengths varied during rotation. The same was observed at the Fermi level.

As all calculations so far served a proof-of-principle concept, these were performed *in vacuo*. Following those, we have added the solvent in form of only water molecules at a first approximation. As a first observation, the inclusion of water significantly increases the dynamic behavior of the whole system. Based on the variation of the hydrogen bond distance with time, we could extract the time evolution of the conductance variation of the functionalized device. Strong fluctuations were observed, but the average value of the conductance with time was more or less kept constant. In this respect, despite the fluctuations, on average and for a given nucleotide the device can output a certain conductance. It remains to be shown, how strong the nucleotide-specificity of this value is if more effects, like the presence of ions are included. In view of novel nanopore sequencing techniques, this work demonstrates the potential of functionalized electrode embedded in a nanopore as efficient DNA detectors. This is based on their nucleotide specific binding to DNA, which was clearly observed in this work. In order to further evaluate all the aspects of these nanopores and their

biosensitivity, further studies should be directed towards a more detailed investigation of the dynamics and solvent effects. The influence of certain salt solutions, as well as extrapolating to longer DNA lengths, and tuning the nanopore-DNA interactions would be necessary in order to evaluate the errors in the signals used to eventually detect the sequence of a DNA passing through a functionalized nanopore.

All authors greatly acknowledge financial support from the collaborative network SFB 716 "Dynamic simulations of systems with large particle numbers" funded by the German Funding Agency (Deutsche Forschungsgemeinschaft-DFG). G.S. and M.F. also thank R. Amorim and R. Scheicher for a fruitful collaboration. This research was supported in part by the bwHPC initiative and the bwHPC-C5 project provided through associated compute services of the JUSTUS HPC facility at the University of Ulm. The bwHPC and bwHPC-C5 (http://www.bwhpc-c5.de) are funded by the Ministry of Science, Research and the Arts Baden-Württemberg (MWK) and the German Research Foundation (DFG). Part of this work was performed on the computational resource ForHLR Phase I/II funded by the Ministry of Science, Research and the Arts Baden-Württemberg and DFG.

References

1. D. Branton, D.W. Deamer, A. Marziali, H. Bayley, S.A. Benner, T. Butler, M. Di Ventra, S. Garaj, A. Hibbs, X. Huang, et al., Nat. Biotechnol. **26**, 1146 (2008)
2. B.M. Venkatesan, R. Bashir, Nat. Nanotechnol. **6**, 615 (2011)
3. R.H. Scheicher, A. Grigoriev, R. Ahuja, J. Mater. Sci. **47**, 7439 (2012)
4. M. Fyta, J. Phys.: Condens. Matter **27**, 273101 (2015)
5. S. Agah, M. Zheng, M. Pasquali, A.B. Kolomeisky, J. Phys. D: Appl. Phys. **49**, 413001 (2016)
6. C. Dekker, Nat. Nanotechnol. **2**, 209 (2007)
7. M. Zwolak, M. Di Ventra, Rev. Mod. Phys. **80**, 141 (2008)
8. M. Di Ventra, M. Taniguchi, Nat. Nano. **11**, 117 (2016)
9. M. Zwolak, M. Di Ventra, Nano. Lett. **5**, 421 (2005)
10. J. Lagerqvist, M. Zwolak, M. Di Ventra, Nano. Lett. **6**, 779 (2006)
11. H. He, R.H. Scheicher, R. Pandey, A. Reily Rocha, S. Sanvito, A. Grigoriev, R. Ahuja, S. Karna, J. Phys. Chem. C **112**, 3456 (2008)
12. F. Patolsky, A. Lichtenstein, I. Willner, Nat. Biotechnol. **19**, 253 (2001)
13. E.M. Boon, D.M. Ceres, T.G. Drummond, M.G. Hill, J.K. Barton, Nat. Biotechnol. **18**, 1096 (2000)
14. C. Merstorf, B. Cressiot, M. Pastoriza-Gallego, A. Oukhaled, J.M. Betton, L. Auvray, J. Pelta, ACS Chem. Biol. **7**, 652 (2012)
15. A.C. Rajan, M.R. Rezapour, J. Yun, Y. Cho, W.J. Cho, S.K. Min, G. Lee, K.S. Kim, ACS Nano. **8**, 1827 (2014)
16. M. Murtaza, S.J. Dawson, D.W. Tsui, D. Gale, T. Forshew, A.M. Piskorz, C. Parkinson, S.F. Chin, Z. Kingsbury, A.S. Wong, et al., Nature **497**, 108 (2013)
17. S. Huang, J. He, S. Chang, P. Zhang, F. Liang, S. Li, M. Tuchband, A. Fuhrmann, R. Ros, S. Lindsay, Nat. Nanotechnol. **5**, 868 (2010)
18. G. Sivaraman, R.G. Amorim, R.H. Scheicher, M. Fyta, Nanoscale **8**, 10105 (2016)
19. W.A. Clay, J.E.P. Dahl, R.M.K. Carlson, N.A. Melosh, Z.X. Shen, Rep. Prog. Phys. **78**, 016501 (2015)
20. J. Dahl, S. Liu, R. Carlson, Science **299**, 96 (2003)
21. W.L. Yang, J.D. Fabbri, T.M. Willey, J.R.I. Lee, J.E. Dahl, R.M.K. Carlson, P.R. Schreiner, A.A. Fokin, B.A. Tkachenko, N.A. Fokina, et al., Science **316**, 1460 (2007)
22. M. Vörös, T. Demjén, T. Szilvási, A. Gali, Phys. Rev. Lett. **108**, 267401 (2012)
23. A.A. Fokin, B.A. Tkachenko, P.A. Gunchenko, D.V. Gusev, P.R. Schreiner, Chem. Eur. J. **11**, 7091 (2005)

24. M.A. Gunawan, J.C. Hierso, D. Poinsot, A.A. Fokin, N.A. Fokina, B.A. Tkachenko, P.R. Schreiner, New J. Chem. **38**, 28 (2014)
25. Y. Zhou, A.D. Brittain, D. Kong, M. Xiao, Y. Meng, L. Sun, J. Mater. Chem. C **3**, 6947 (2015)
26. A. Spasov, T. Khamidova, L. Bugaeva, I. Morozov, Pharm. Chem. J. **34**, 1 (2000)
27. F.C. Maier, G. Sivaraman, M. Fyta, Eur. Phys. J. E **37**, 95 (2014)
28. A. Nazem, G. Mansoori, J. Bioanal. Biomed. **6**, 9 (2014)
29. B. Reisberg, R. Doody, A. Stöffler, F. Schmitt, S. Ferris, H.J. Möbius, New England J. Med. **348**, 1333 (2003)
30. D.M. Robinson, G.M. Keating, Drugs **66**, 1515 (2006)
31. M.W. Schmidt, K.K. Baldridge, J.A. Boatz, S.T. Elbert, M.S. Gordon, J.H. Jensen, S. Koseki, N. Matsunaga, K.A. Nguyen, S. Su, et al., J. Comput. Chem. **14**, 1347 (1993)
32. M.S. Gordon, M.W. Schmidt, in *Theory and applications of computational chemistry*, edited by C.E. Dykstra, G. Frenking, K.S. Kim, G.E. Scuseria (Elsevier, Amsterdam, 2005), pp. 1167–1189
33. J.M. Soler, E. Artacho, J.D. Gale, A. Garcia, J. Junquera, P. Ordejon, D. Sánchez-Portal, J. Phys.: Condens. Matter **14**, 2745 (2002)
34. Y. Zhao, D.G. Truhlar, Acc. Chem. Res. **41**, 157 (2008)
35. H. Vovusha, S. Sanyal, B. Sanyal, J. Phys. Chem. Lett. **4**, 3710 (2013)
36. D. Umadevi, G.N. Sastry, J. Phys. Chem. Lett. **2**, 1572 (2011)
37. D. Branton, D.W. Deamer, A. Marziali, H. Bayley, S.A. Benner, T. Butler, M. Di Ventra, S. Garaj, A. Hibbs, X. Huang, et al., Nat. Biotechnol. **26**, 1146 (2008)
38. V.R. Cooper, T. Thonhauser, D.C. Langreth, J. Chem. Phys. **128**, 204102 (2008)
39. S.F. Boys, F.d. Bernardi, Mol. Phys. **19**, 553 (1970)
40. J.P. Perdew, K. Burke, M. Ernzerhof, Phys. Rev. Lett. **77**, 3865 (1996)
41. K. Stokbro, J. Taylor, M. Brandbyge, O. Pablo, Ann. N.Y. Acad. Sci. **1006**, 212 (2003)
42. J. Hutter, M. Iannuzzi, F. Schiffmann, J. VandeVondele, Wiley Interdiscip. Rev.: Comput. Mol. Sci. **4**, 15 (2014)
43. S. Goedecker, M. Teter, J. Hutter, Phys. Rev. B **54**, 1703 (1996)
44. C. Hartwigsen, S. Goedecker, J. Hutter, Phys. Rev. B **58**, 3641 (1998)
45. J. VandeVondele, J. Hutter, J. Chem. Phys. **127**, 114105 (2007)
46. S. Grimme, J. Antony, S. Ehrlich, H. Krieg, J. Chem. Phys. **132**, 154104 (2010)
47. S.M. Foiles, M.I. Baskes, M.S. Daw, Phys. Rev. B **33**, 7983 (1986)
48. S. Plimpton, J. Comput. Phys. **117**, 1 (1995)
49. N. Sändig, F. Zerbetto, Chem. Commun. **46**, 667 (2010)
50. F. Maseras, K. Morokuma, J. Comput. Chem. **16**, 1170 (1995)
51. J. Pu, J. Gao, D.G. Truhlar, ChemPhysChem **6**, 1853 (2005)
52. D. Golze, M. Iannuzzi, M.T. Nguyen, D. Passerone, J. Hutter, J. Chem. Theory Comput. **9**, 5086 (2013)
53. C.S. Sarap, P. Partovi-Azar, M. Fyta, ACS Appl. Bio Mater. **1**, 59 (2018)
54. M. Barbatti, A.J.A. Aquino, H. Lischka, Phys. Chem. Chem. Phys. **12**, 4959 (2010)
55. D. Varsano, R. Di Felice, M.A.L. Marques, A. Rubio, J. Phys. Chem. B **110**, 7129 (2006)
56. S.K. Min, W.Y. Kim, Y. Cho, K.S. Kim, Nat. Nanotechnol. **6**, 162 (2011)
57. P. Krstić, B. Ashcroft, S. Lindsay, Nanotechnology **26**, 084001 (2015)